MULTICLUSTERING AND PHYSICS OF EXOTIC NUCLEAR SHAPES*

W. NAZAREWICZ[a,b,c,d], S. ĆWIOK[d,e], J. DOBACZEWSKI[c]

AND J.X. SALADIN[e]

[a] Joint Institute for Heavy Ion Research and Physics Division
Oak Ridge National Laboratory
P.O. Box 2008, Oak Ridge, TN 37831, U.S.A.

[b] Department of Physics, University of Tennessee
Knoxville, TN 37996, U.S.A.

[c] Institute of Theoretical Physics, Warsaw University
Hoża 69, PL-00681, Warsaw, Poland

[d] Institute of Physics, Warsaw University of Technology,
Koszykowa 75, PL-00662 Warsaw, Poland

[e] University of Pittsburgh, Pittsburgh, PA 15260, U.S.A.

(Received November 14, 1994)

The importance of the ground-state shell structure for the formation and stability of excited exotic nuclear configurations is discussed in terms of the multicluster model based on dynamical symmetries of a three-dimensional harmonic oscillator. As a spectacular example, it is shown that the density distribution at the third hyperdeformed minimum in the actinide nuclei resembles a di-nucleus consisting of a nearly-spherical fragment around the doubly-magic ^{132}Sn, and a well-deformed fragment from the neutron-rich $A \sim 100$ region.

PACS numbers: 21.60.Cs

---

* Presented at the XXIX Zakopane School of Physics, Zakopane, Poland, September 5–14, 1994.

1. Introduction

The observation of superdeformed (SD) and hyperdeformed (HD) states constitutes an important confirmation of the shell structure of the nucleus. The unusual stability of spherical, SD, and HD states can be attributed to strong shell effects that are present in the average nuclear potential. Theoretically, the variation in the single-particle level density with shell filling (the level bunching), the existence of spherical and deformed magic numbers, and the unusual shell stability of certain shapes has a beautiful interpretation in terms of semiclassical periodic orbits [1–4]. Indeed, the single-particle level density,

$$g(\epsilon) = \sum_i \delta(\epsilon - \epsilon_i)\,, \tag{1}$$

and the shell energy can be expressed [5] as a sum over semiclassical periodic orbits. Consequently, the shell structure of a many-body system (and hence the presence or absence of large deformations) has its deep roots in the nonlinear dynamics of the corresponding classical Hamiltonian and the geometry of classical orbits [1, 4, 6].

For the harmonic oscillator model, often discussed in the context of the SD and HD shell structures [7, 8], the strongest level degeneracy occurs when the frequency ratio is a rational number; this leads to an appearance of deformed magic gaps and magic numbers [1, 4, 9]. In spite of many differences [4], the shell-energy pattern of a realistic average potential (including the flat-bottom effect and the spin-orbit term) also leads to the stabilization of SD and HD shapes.

In quantum-mechanical systems, strong shell effects (*i.e.*, degeneracies) seldom happen by chance; they reflect the presence of dynamical (self-consistent) symmetries of the Hamiltonian. This offers additional quantum numbers associated with the underlying dynamical symmetry which are the eigenvalues of the Casimir operators of the corresponding symmetry group (*i.e.*, the local constants of motion). In this respect, the problem of degeneracies of the single-particle levels of a three-dimensional harmonic oscillator with frequencies in rational ratios (rational harmonic oscillator, RHO) has very interesting properties. These are briefly reviewed in Section 2. Generic SD and HD quantum numbers of the RHO offer a possibility to invoke a concept of "multiclustering" (Sec. 3). Experimental consequences of the multicluster model are discussed in Sec. 4 (light nuclei) and Sec. 5 (actinides).

2. Symmetries of the rational harmonic oscillator

One of the simplest but, at the same time, one of the most transparent and powerful models of nuclear structure is the harmonic oscillator model. Especially in light nuclei, where both the spin-orbit and Coulomb interactions are weak, and the diffuseness of the nuclear surface is comparable with the nuclear radius, the harmonic oscillator model gives a fairly good approximation to the nuclear average potential.

The single-particle Hamiltonian of the three-dimensional oscillator potential is given by

$$\hat{H} = \tfrac{1}{2}\sum_{i=1}^{3}(p_i^2 + \omega_i^2 x_i^2) = \tfrac{1}{2}\sum_{i=1}^{3}\omega_i\{a_i, a_i^+\}\,, \tag{2}$$

(here, and in the following we assume the nucleon mass m=1 and $\hbar$=1).

The single-particle energies of (2) are

$$e_{n_1,n_2,n_3} = \sum_{i=1}^{3}\omega_i\left(n_i + \tfrac{1}{2}\right)\,, \tag{3}$$

where n_i are the numbers of oscillator quanta in three spatial directions, and the corresponding Hilbert space, $\mathcal{H}$, is spanned by the kets

$$|\hat{n}\rangle = |n_1 n_2 n_3\rangle = \frac{1}{\sqrt{n_1!n_2!n_3!}}(a_1^+)^{n_1}(a_2^+)^{n_2}(a_3^+)^{n_3}|-\rangle\,. \tag{4}$$

A single-particle diagram of the axially-deformed harmonic oscillator is displayed in Fig. 1.

The general case of the quantal many-dimensional RHO was investigated by Vendramin [10], Maiella and Vilasi [11], and Quesne [12]. (The case of only one rational frequency ratio or no rational frequency ratio was discussed in Ref. [12].) They derived the canonical transformation and introduced the generalized Bose operators (see also Refs [13, 14]). In the context of nuclear physics, the connection between the symmetry algebra of the RHO and nuclear superdeformation has been pointed out and discussed in Refs [15–17] where more references to other papers on the symmetries of the RHO can be found.

2.1. Generalized Bose operators

For the RHO, the ratios of oscillator frequencies are rational numbers. This can be expressed in terms of three integers k_i, $i = 1, 2, 3$:

$$\omega_i k_i = \tilde{\omega}\,, \tag{5}$$

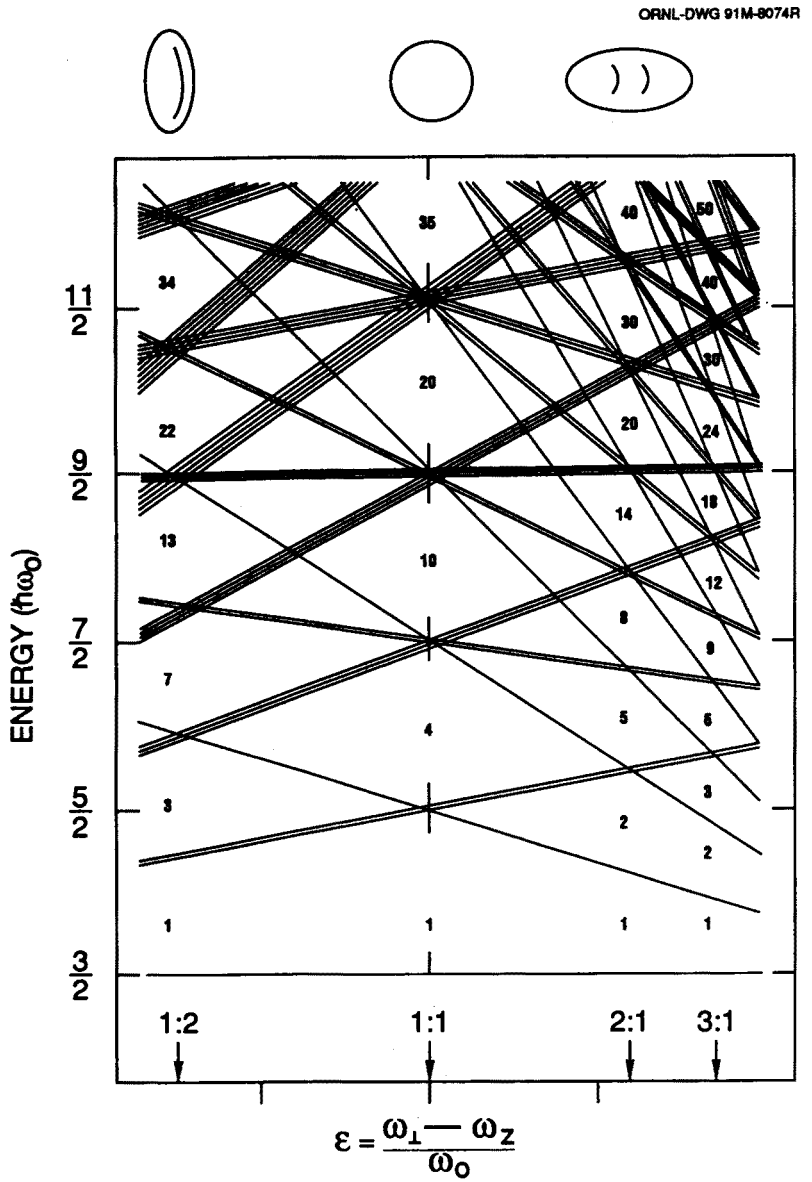

Fig. 1. Single-particle level spectrum of the axially symmetric harmonic oscillator ($\omega_1{=}\omega_2{=}\omega_\perp$) in units of $\omega_o = \frac{1}{3}(2\omega_\perp + \omega_3)$ shown as a function of quadrupole deformation, $\varepsilon{=}(\omega_\perp{-}\omega_3)/\omega_o$. Due to the axial symmetry, the single-particle energies depend only on two quantum numbers: $n_\perp{\equiv}n_1{+}n_2$ and n_3. The orbital degeneracy is $n_\perp{+}1$, which is illustrated by artificially splitting the lines. The arrows indicate the characteristic deformations corresponding to the ratio of $\omega_\perp : \omega_3 = 1:2, 1:1, 2:1$, and $3:1$.

where $\tilde{\omega}$ can be calculated from the volume conservation condition, $\omega_1\omega_2\omega_3 = \tilde{\omega}_0^3$, and is equal to

$$\tilde{\omega} = \sqrt[3]{k_1k_2k_3}\cdot\tilde{\omega}_0, \quad \tilde{\omega}_0 = \frac{41}{A^{1/3}}. \tag{6}$$

For example, the spherical shape corresponds to $k_1{=}k_2{=}k_3$, while the axial shapes have $k_1{=}k_2{=}k_\perp$. In the axial case, it is convenient to write the single-particle energies in terms of the shell frequency, ω_{shell}, and the shell principal quantum, N_{shell}, defined by [1]:

$$\omega_\perp n_\perp + \omega_3 n_3 = \omega_{\mathrm{shell}} N_{\mathrm{shell}}, \quad N_{\mathrm{shell}} = n_\perp k_3 + n_3 k_\perp, \quad \omega_{\mathrm{shell}} = \frac{\tilde{\omega}}{k_\perp k_3}. \tag{7}$$

Let us now introduce new quantum numbers ν_i and λ_i:

$$n_i = k_i\nu_i + \lambda_i, \quad \nu_i = \left[\frac{n_i}{k_i}\right], \quad \lambda_i = n_i\,(\mathrm{mod}\,k_i), \tag{8}$$

where the symbol $[x]$ stands for the integer part of x. Single-particle energies of the RHO can be thus written as

$$e_{M;\lambda_1\lambda_2\lambda_3} = \tilde{\omega}M + \tilde{\omega}\sum_{i=1}^{3}\frac{\lambda_i + \frac{1}{2}}{k_i}, \tag{9}$$

where

$$M = \nu_1 + \nu_2 + \nu_3 \tag{10}$$

is the *new principal quantum number.* At fixed values of λ_i, the level degeneracy is equal to $\frac{1}{2}(M+1)(M+2)$; *i.e.*, it corresponds exactly to the degeneracy of the spherical oscillator with principal quantum number M. This fact suggests that the "hidden" symmetry of the quantum-mechanical RHO should be exactly the same as the dynamical SU(3) symmetry of the isotropic harmonic oscillator. In order to demonstrate this explicitly, one can introduce new ladder operators [14]

$$\begin{aligned} A_i^{\{\lambda\}} &= \frac{1}{\sqrt{k_i}}(a_i)^{k_i}\left(\frac{\hat{n}_i - \lambda_i}{\hat{n}_i(\hat{n}_i-1)\ldots(\hat{n}_i-k_i+1)}\right)^{\frac{1}{2}} \\ &= (a_i)^{k_i}\left(\left[\frac{\hat{n}_i}{k_i}\right]\frac{(\hat{n}_i-k_i)!}{\hat{n}_i!}\right)^{\frac{1}{2}}, \end{aligned} \tag{11}$$

where $\hat{n}_i{=}a_i^+a_i$ is the boson number operator and $\{\lambda\}\equiv(\lambda_1\lambda_2\lambda_3)$. It is easy to verify that operators (11) indeed fulfill the standard boson commutation rules, *i.e.*

$$\left[A_i^{\{\lambda\}}, A_j^{\{\lambda\}+}\right] = \delta_{i,j}. \tag{12}$$

The new boson operator, $A_i^{\{\lambda\}}$, acts only on the quantum number, ν_i, and leaves λ_i unchanged, *i.e.*,

$$A_j^{\{\lambda\}+}|\cdots,\nu_i k_i+\lambda_i,\cdots\rangle=\sqrt{\nu_i+1}|\cdots,(\nu_i+1)k_i+\lambda_i,\cdots\rangle\,. \tag{13}$$

This means that the Hilbert space of the RHO can be decomposed as

$$\mathcal{H}=\oplus_{\{\lambda\}}\mathcal{H}^{\{\lambda\}}, \tag{14}$$

where the subspace $\mathcal{H}^{\{\lambda\}}$ is spanned by kets (4) with a fixed value of $\{\lambda\}$. In this new subspace, the RHO Hamiltonian becomes

$$\hat{H}=\tfrac{1}{2}\tilde{\omega}\sum_{i=1}^{3}\left\{A_i^{\{\lambda\}},A_i^{\{\lambda\}+}\right\}-\tfrac{1}{2}\sum_{i=1}^{3}\omega_i(k_i-2\lambda_i-1)\,, \tag{15}$$

i.e., it formally looks like the Hamiltonian of the isotropic harmonic oscillator (up to an additive constant). Now, analogous to the spherical case, one can construct eight generators linear in $\left\{A_i^{\{\lambda\}},A_i^{\{\lambda\}+}\right\}$ that fulfill the commutation rules of SU(3) and commute with the Hamiltonian (15). This completes proof that SU(3) is indeed the dynamical symmetry in question.

2.2. Classification of eigenstates of the RHO

The RHO eigenstates belonging to the same $\{\lambda\}$ family form (for a given M) the basis of an irreducible symmetric representation (irrep) of SU(3). Each family has a corresponding ground state belonging to the one-dimensional representation of SU(3) for $M=0$, which is the vacuum for the new bosons (11). Because of the condition

$$0\le\lambda_i<k_i\,, \tag{16}$$

the number of $\{\lambda\}$-families is equal to $k_1k_2k_3$ and becomes large when the frequency ratios are not very commensurable. As an example, Fig. 2 shows the RHO spectrum in the case of $k_1=1$, $k_2=2$, $k_3=3$. The levels can be grouped into six independent $\{\lambda\}$-families, each forming the isotropic oscillator spectrum with frequency $\tilde{\omega}$.

At the spherical shape, $k_1=k_2=k_3=1$, there is only one family present labeled by $\{\lambda\}=(000)$. The degeneracy of each level is $\frac{1}{2}(M+1)(M+2)$ and the magic gaps occur at particle numbers[1]

$$N_M=\tfrac{1}{6}(M+1)(M+2)(M+3)=1,\ 4,\ 10,\ 20,\ 35,\ 56,\ 84,\ \cdots, \tag{17}$$

[1] Here, and in the following, we give magic numbers for the RHO only, *i.e.*, without including the two-fold spin degeneracy.

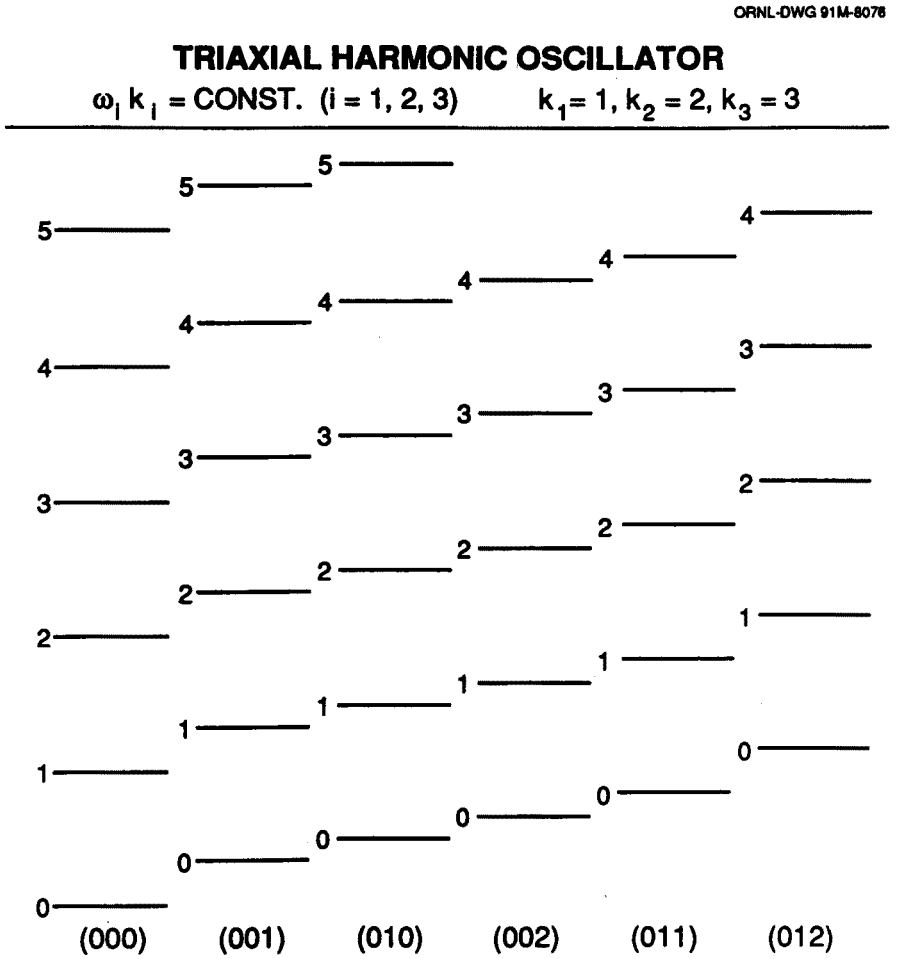

Fig. 2. Spectrum of the RHO with k_1=1, k_2=2, k_3=3. Each level is labeled by means of the principal quantum number M and quantum numbers $(\lambda_1\lambda_2\lambda_3)$ that label different irreducible representations of SU(3). Except the usual SU(3) degeneracy, $\frac{1}{2}(M+1)(M+2)$, no additional degeneracies are present.

for M=0, 1, 2, $\cdots$, respectively. Other cases of significant physical interest are the SD prolate (k_1=1, k_2=1, k_3=2) and the HD prolate (k_1=1, k_2=1, k_3=3) shapes. Here, since λ_1=λ_2=0, the number of independent SU(3) irreps for a given M is simply equal to k_3, and they can be easily distinguished by means of λ_3.

2.2.1. Prolate SD and HD shapes

As seen in Fig. 3, there are two kinds of closed-shell systems that are expected at SD shapes. In the "asymmetric" case, indicated as A, the

number of filled shells within the family $\{\lambda\}=(000)$ is larger by one than that within the family $\{\lambda\}=(001)$. Consequently, the magic numbers are then equal to sums of two consecutive spherical magic numbers and read $N_M^{(000)}+N_{M-1}^{(001)} = 1,\ 5,\ 14,\ 30,\ 55,\ etc.$. In the "symmetric" variant B, the missing (001) shell is filled, and the magic numbers are equal to doubled spherical oscillator magic numbers, $N_M^{(000)}+N_M^{(001)} = 2,\ 8,\ 20,\ 40,\ 70,\ etc.$.

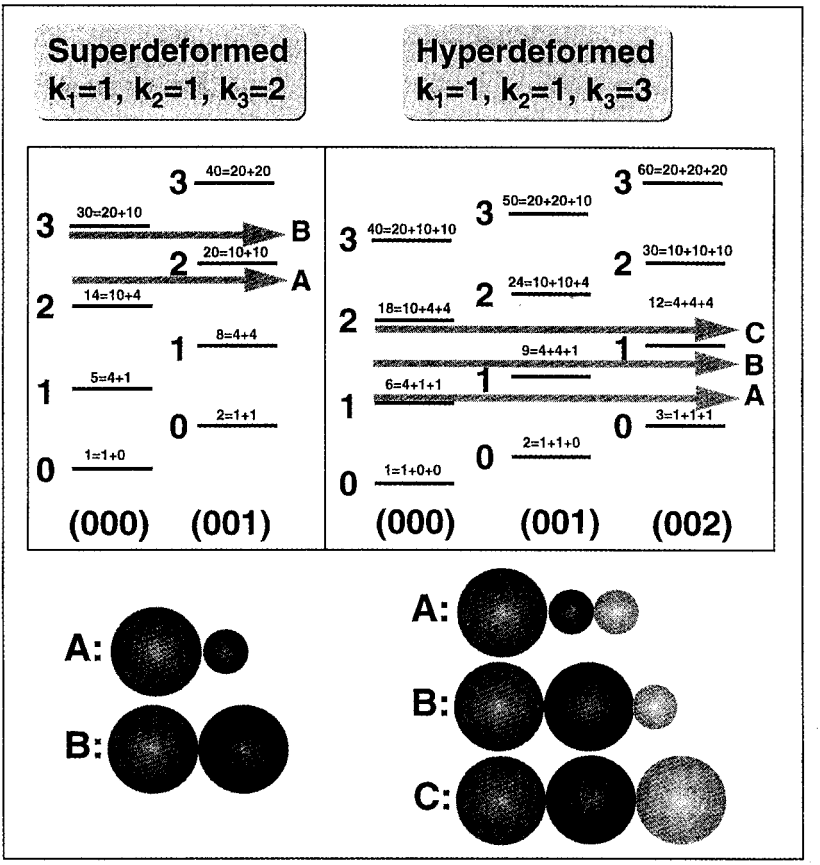

Fig. 3. Spectrum of the RHO with $k_1 = 1$, $k_2 = 1$, and $k_3 = 2$ (SD prolate, left) or $k_3 = 3$ (HD prolate, right). Each level is labeled by the principal quantum number M and quantum numbers $(\lambda_1\lambda_2\lambda_3)$. Except the usual SU(3) degeneracy, $\frac{1}{2}(M+1)(M+2)$, no additional degeneracies are present. Different positions of the Fermi level for closed-shell systems A, B or C are indicated. The schematic diagrams in the bottom portion illustrate the number of occupied particles within each $\{\lambda\}$-family in cases A, B or C.

The situation becomes slightly more complex at HD shapes (see Fig. 3). In the "strongly asymmetric" variant, A, the number of filled shells within

the family (000) is larger by one than those of the families (001) and (002), which leads to magic numbers $N_M^{000} + N_{M-1}^{001} + N_{M-1}^{002} = 1,\ 6,\ 18,\ 40,\ 75,$ *etc.*. In the variant B, the occupation of the family (002) is lower than the occupations of the families (000) and (001), and the resulting magic numbers are $N_M^{000} + N_M^{001} + N_{M-1}^{002} = 2,\ 9,\ 24,\ 50,\ 90,$ *etc.*. Finally, in the "symmetric" case C, the occupations of families (000), (001), and (002) are identical, and the magic numbers are equal to tripled spherical oscillator magic numbers, $N_M^{000} + N_M^{001} + N_M^{002} = 3,\ 12,\ 30,\ 60$ and 105, *etc.*.

2.2.2. Oblate shapes

The examples discussed so far represent the simplest possible situation in which the numbers k_i are relatively prime. The degeneracy pattern becomes, however, rather complicated in the case when two k_i's have a common multiplier. Let us consider, for instance, the case of oblate SD shapes with $k_1 = k_2 = k_\perp > 1$, $k_3 = 1$. The number of one-dimensional irreps of SU(3) is equal to $k_\perp^2$ ($0 \leq \lambda_1 < k_1$, $0 \leq \lambda_2 < k_2$, $\lambda_3 = 0$), and the eigenstates (9) are given by:

$$e_{M,\lambda_1\lambda_20} = \tilde{\omega}(M + \tfrac{1}{2}) + \tilde{\omega}\left(\frac{\lambda_1 + \lambda_2 + 1}{k_\perp}\right). \tag{18}$$

It is seen that, due to the equality of energies,

$$e_{M,\lambda_1\lambda_20} = e_{M';\lambda_1'\lambda_2'0}\,, \tag{19}$$

which occurs for

$$M' = M + \left[\frac{\lambda_1 + \lambda_2}{k_\perp}\right] \quad \text{and} \quad \lambda_1' + \lambda_2' = \lambda_1 + \lambda_2 (\mathrm{mod}\ k_\perp)\,, \tag{20}$$

additional degeneracies, not accounted for by the dynamical SU(3) symmetry, are present. Fig. 4 shows the single-particle spectrum of the RHO for $k_\perp = 2$. According to Eq. (19), the levels belonging to pairs of irreps $(M, 010)$–$(M, 100)$ and $(M+1, 000)$–$(M, 110)$ are degenerate. The degeneracy of the energy levels (in the discussed case: 1, 2, 4, 6, 9, $\cdots$) does not coincide with the dimension of any irrep of SU(3).

In Ref. [11] it was demonstrated that, except for particular cases, each energy level of the RHO corresponds to a reducible (rrep) representation of SU(3). In order to label the rreps of SU(3), one can introduce quantum numbers $\lambda_\perp$ and $\tilde{N}$, defined in a similar way as λ_i (see, *e.g.*, Ref. [8]):

$$\lambda_\perp = \nu_\perp (\mathrm{mod}\, k_\perp), \quad \tilde{N} = \nu_\perp + \nu_3\,, \tag{21}$$

SUPERDEFORMED OBLATE
$k_1 = 2, k_2 = 2, k_3 = 1$

N_{SHELL}		DEGEN.	IRREP SU(3) $(M, \lambda_1\lambda_2\lambda_3)$	RREP SU(3) $(\tilde{N}, \lambda_\perp)$	IRREP O(4) (j^+, j^-)
4	———	9	(1,110), (2,000)	(2, 0)	(1, 1)
3	———	6	(1,010), (1,100)	(1, 1)	$(1, \frac{1}{2})$
2	———	4	(0,110), (1,000)	(1, 0)	$(\frac{1}{2}, \frac{1}{2})$
1	———	2	(0,100), (0,010)	(0, 1)	$(\frac{1}{2}, 0)$
0	———	1	(0,000)	(0, 0)	(0, 0)

Fig. 4. Spectrum of the RHO with $k_1 = k_2 = 2$, $k_3 = 1$ (SD oblate shape). The principal shell quantum number N_{shell} is defined by means of Eq. (7). Each level is labeled by means of the irrep SU(3) labels $(M, \lambda_1\lambda_2\lambda_3)$, the rrep SU(3) labels $(\tilde{N}, \lambda_\perp)$, and the irrep O(4) labels (j^+, j^-) (see text).

where $\nu_\perp = [n_\perp/k_\perp]$. Contrary to the case of prolate shapes, the shell degeneracy depends explicitly on $\lambda_\perp$:

$$n(\tilde{N}, \lambda_\perp) = \tfrac{1}{2}(\tilde{N} + 1)[k_\perp \tilde{N} + 2(\lambda_\perp + 1)]\,. \tag{22}$$

(For the general case of $k_3 \neq 1$, see Ref. [10].) The total number of states in an oblate SD magic system [counting from the bottom and including the last $(\tilde{N}, \lambda_\perp)$ shell] is then equal [18]:

$$\begin{aligned} N_{\tilde{N},\lambda_\perp} =& \tfrac{1}{2}(\lambda_\perp + 1)(\lambda_\perp + 2) N_{\tilde{N}} \\ &+ \left[\tfrac{1}{2}k_\perp(k_\perp - 1) + (\lambda_\perp + 2)(l - \lambda_\perp - 1)\right] N_{\tilde{N}-1} \\ &+ \tfrac{1}{2}(k_\perp - \lambda_\perp - 1)(l - \lambda_\perp - 2) N_{\tilde{N}-2}\,, \end{aligned} \tag{23}$$

where $N_{\tilde{N}}$ is given by Eq. (17). In the particular case of $k_\perp = 2$, the third term in Eq. (23) vanishes, and the magic numbers can thus be divided into two groups with $\lambda_\perp = 0$ or 1

$$N_{\tilde{N},\lambda_\perp} = \begin{cases} N_{\tilde{N}} + 3N_{\tilde{N}-1} = 1, 7, 22, 50, \cdots & \text{if} \quad \lambda_\perp = 0 \\ 3N_{\tilde{N}} + N_{\tilde{N}-1} = 3, 13, 34, \cdots & \text{if} \quad \lambda_\perp = 1\,. \end{cases}$$

It has been noticed in Ref. [19] that the imposition of a reflection condition can change SU(3) to O(4), and vice versa. To see the connection, let us consider the isotropic harmonic oscillator with an impenetrable barrier across the symmetry (say, xy) plane. The eigenstates of the problem are the odd-n_3 oscillator states. There are listed in portion (b) of Table I, while

the states with even z-parity are given in portion (c). The degeneracy patterns of both n_3-even and n_3-odd sets are the same and are *exactly equal* to the degeneracy of SD oblate states in Fig. 4. The analogy between the structure of SD oblate states with $k_\perp = 2$, and the harmonic oscillator with the barrier, is by no means accidental. Indeed, the N_{shell} quantum number (7) in the discussed case is equal to

$$N_{\text{shell}} = n_1 + n_2 + 2n_3 = n_\perp + n_3' = N', \tag{24}$$

where $n_3' = 2n_3$ is always even and N' is the principal quantum number of the oscillator with the barrier.

TABLE I

States of the spherical harmonic oscillator in representation (4). In (a), "*etc.*" indicates possible permutations of quantum numbers. States in (b) are those remaining after inserting a wall in the xy-plane (n_3-odd), while states in (c) have even values of n_3. The degeneracy of the level is contained in the first column (*cf.* Ref. [19]).

Degeneracy	Cartesian representation of states
	(a) Full three-dimensional oscillator
21	500 *etc.*, 410 *etc.*, 320 *etc.*, 311 *etc.*, 221 *etc.*
15	400 *etc.*, 310 *etc.*, 220 *etc.*, 211 *etc.*
10	300 *etc.*, 210 *etc.*, 111
6	200 *etc.*, 110 *etc.*
3	100 *etc.*
1	000
	(b) n_3-odd states
9	005, 041, 401, 023, 203, 311, 131, 113, 221
6	301, 031, 103, 013, 211, 121
4	003, 201, 021, 111
2	101, 011
1	001
	(c) n_3-even states
12	500, 050, 410, 140, 104, 014, 320, 230, 302, 032, 212, 122
9	400, 040, 004, 310, 130, 220, 022, 202, 112
6	300, 030, 210, 120, 102, 012
4	200, 020, 002, 110
2	100, 010
1	000

The resulting degeneracy pattern can be associated [19, 12] with two interleaving sets of irreps of O(4). The generators of O(4) are two vectors $\boldsymbol{J}$ and $\boldsymbol{K}$ generating rotations in the four-dimensional plane. By introducing

two vector operators $\boldsymbol{J}^{\pm} = \frac{1}{2}(\boldsymbol{J} \pm \boldsymbol{K})$, one can label the irreps of O(4) using two quantum numbers j^+ and j^-. The corresponding dimensionality is $(2j^+ + 1)(2j^- + 1)$. The eigenstates of a SD oblate RHO with $k_\perp = 2$ form the basis for two irreps of O(4). Square irreps with $j^+ = j^- = \frac{1}{4}N_{\text{shell}}$ arise when N_{shell} is even, while rectangular ones with $j^+ = j^- + \frac{1}{2} = \frac{1}{4}(N_{\text{shell}} + 1)$ correspond to even values of N_{shell}. The values of j^+ and j^- can be expressed in terms of $\tilde{N}$ and $\lambda_\perp$ as

$$j^+ = \tfrac{1}{2}(\tilde{N} + \lambda_\perp), \quad j^- = \tfrac{1}{2}\tilde{N}, \tag{25}$$

see Fig. 4.

2.3. *Selection rules*

The degenerate shell of the RHO consists, in general, of states having different parities. Indeed, the generalized Bose operators (11) are parity-even for even values of k_i and parity-odd for odd values of k_i:

$$\hat{\pi} A_i^{\{\lambda\}} \hat{\pi}^{-1} = (-1)^{k_i} A_i^{\{\lambda\}}. \tag{26}$$

Consequently, the total parity of the single-particle state $|\hat{n}\rangle$ can be written as

$$\pi_{\hat{n}} = (-1)^N = (-1)^{\lambda_1+\lambda_2+\lambda_3}(-1)^{k_1\nu_1+k_2\nu_2+k_3\nu_3} = \pi_\lambda \pi_\nu . \tag{27}$$

The above expression can be given a simple interpretation. The parity π_λ is the intrinsic parity of the corresponding bosonic vacuum, while π_ν represents the parity of an excited mode. In the case of SD prolate shapes with even values of k_3, Eq. (27) reduces to

$$\pi_{\hat{n}} = (-1)^{\lambda_3}(-1)^{n_\perp} = (-1)^{\lambda_3 + \Lambda}, \tag{28}$$

where Λ is the projection of the orbital angular momentum on the symmetry axis (z-axis).

The fact that degenerate single-particle orbitals have different parities has interesting consequences for the octupole mode, $Q_{3K} = r^3 Y_{3K}$, since the optimum condition for the level hybridization is met. Table II shows the energies of particle-hole excitations associated with various components of the octupole tensor [20, 21]. Let us first consider the SD shape with $k_\perp = 1$ and $k_3 = 2$. The $K = 1$ and $K = 3$ octupole components conserve intrinsic parity π_λ. Interestingly, since $\Delta E = 2\omega_3 - \omega_\perp = 0$ for $K = 1$, there exist nonvanishing matrix elements between states belonging to the same supershell. The $K = 0$ and $K = 2$ interactions act only between states with opposite values of π_λ. At the SD oblate shape with $k_\perp = 2$, $k_3 = 1$,

this scenario is reversed, *i.e.*, the $K = 0$ and $K = 2$ modes conserve π_λ. By inspecting Table II, one can immediately conclude that the SD oblate nuclei should be unstable with respect to $K = 0$ and $K = 2$ octupole fields ($\Delta E = 2\omega_\perp - \omega_3 = 0$).

TABLE II

Energies of the particle-hole excitation, ΔE, associated with the octupole double-stretched interaction Q''_{3K}.

K	$\Delta E/\hbar$	Optimal conditions for instability
0	ω_3, $2\omega_\perp - \omega_3$, $2\omega_\perp + \omega_3$, $3\omega_3$	superdeformed oblate shapes
1	$\omega_\perp$, $2\omega_3 - \omega_\perp$, $2\omega_3 + \omega_\perp$, $3\omega_\perp$	superdeformed prolate shapes
2	ω_3, $2\omega_\perp - \omega_3$, $2\omega_\perp + \omega_3$	superdeformed oblate shapes
3	$\omega_\perp$, $3\omega_\perp$	no instability

The fact that the elementary modes of the RHO are nothing else but the SU(3) bosons has deep theoretical consequences, since calculations at SD shapes can be greatly simplified by introducing new, *symmetry-adapted* operators constructed by means of new coordinates and momenta:

$$X_i^{\{\lambda\}} = \frac{1}{\sqrt{2}}\left(A_i^{\{\lambda\}} + A_i^{\{\lambda\}+}\right), \qquad P_i^{\{\lambda\}} = \frac{1}{i\sqrt{2}}\left(A_i^{\{\lambda\}} - A_i^{\{\lambda\}+}\right). \quad (29)$$

3. Multicluster model and shell effects

According to Eq. (7), the energy difference between neighboring oscillator shells, $\tilde{\omega}_{\mathrm{shell}}$, decreases smoothly with deformation. This indicates that the overall magnitude of the shell effects is expected to be strongest at the spherical shape. However, as indicated by some examples discussed below, even at very strong elongations, the appearing shell structure leads to an enhanced stability as in the case of spherical shell gaps. Moreover, we will describe the deformed shell-stabilized systems in terms of "multiclusters" of spherical subsystems (clusters), as dictated by the decomposition of the RHO representations into the isotropic ones, described in the previous section. Of course, the term "cluster" should not be understood in the most direct sense of a spatial spherical cluster since, in medium mass and heavy nuclei, the probability of clustering into large fragments is strongly inhibited by the Pauli principle. However, it turns out that the group theory symmetries of these clusters induce some properties of SD states as if the clustering occurred in the real space. The main assumption of the "cluster" model is that every $\{\lambda\}$-family [an SU(3) oscillator] should correspond to

an independent fragment. The number of fragments is then equal to the number of one-dimensional irreps of SU(3), *i.e.*, it is equal to $k_1k_2k_3$.

3.1. Multipole vibrations in the RHO model

In order to analyze the multipole couplings in the RHO model, the doubly-stretched multipole-multipole separable interaction of Sakamoto and Kishimoto [22, 23], defined in terms of

$$Q''_{\lambda K} = r''^{3} Y_{\lambda K}(\Omega''), \quad x''_i \equiv \frac{\omega_i}{\omega_0} x_i, \quad (i = 1, 2, 3), \tag{30}$$

has been used. This interaction can be viewed as an improved conventional multipole-multipole force. Firstly, it satisfies the nuclear self-consistency rigorously, even if the system is deformed. Secondly, it yields the zero-energy RPA spurious modes, *i.e.*, it automatically separates the translational and reorientation modes. Last, but not least, for the doubly-stretched interaction, the coupling between octupole and dipole modes disappears.

Let us first discuss properties of low-lying multipole modes within the RPA formalism. The RPA equation for the excitation energy, ω, is given by the dispersion relation [20–22]

$$\frac{1}{\kappa^{\rm self}_{\lambda K}} - R_{\lambda K}(\omega) = 0, \tag{31}$$

where $\kappa^{\rm self}_{\lambda K}$ is the self-consistent coupling strength given by Eq. (2.81) in Ref. [22], and

$$R_{\lambda K}(\omega) = \sum_i \frac{E_i - E_0}{(E_i - E_0)^2 - \omega^2} \left[|\langle i|Q''_{\lambda K}|0\rangle|^2 + |\langle i|Q''^{*}_{\lambda K}|0\rangle|^2 \right] \tag{32}$$

is the RPA response function. The value of $R_{\lambda K}(\omega = 0)/2$ is the inverse energy-weighted sum rule, S_{-1}, which can be related to the *microscopic* interaction strength, $\kappa^{\rm mic}_{\lambda K}$, by [22, 24]

$$\frac{1}{\kappa^{\rm mic}_{\lambda K}} = 2S_{-1} = R_{\lambda K}(0). \tag{33}$$

Consequently, if the quantity

$$I_{\lambda K} \equiv (\kappa^{\rm self}_{\lambda K})^{-1} - (\kappa^{\rm mic}_{\lambda K})^{-1} \tag{34}$$

is negative (positive), then the lowest energy multipole mode is unstable (stable) with respect to permanent deformation. In order to check the susceptibility of the RHO to multipole distortions, one can thus calculate $I_{\lambda K}$

as a function of the shell filling. For the RHO this can be done analytically. Results are presented below of the symbolic-language MATHEMATICA© calculations performed for the closed-shell systems. By M and A we denote the number of the RHO quanta (10) in the highest occupied shell and the total number of occupied RHO states, respectively.

3.1.1. Quadrupole modes

(i) **Spherical case.** Here

$$I_{2K}^{\mathrm{sph}} = \frac{15}{32\pi}\frac{1}{\omega_0^3}A(M+2) > 0, \quad K = 0,1,2. \tag{35}$$

It is seen that the spherical magic harmonic oscillator is *stable* with respect to quadrupole distortions, and the result does not depend on K which is a simple consequence of the rotational invariance.

(ii) **Superdeformed case.** The results presented in Table III show that in the symmetric case (B) the spurious $K = 1$ reorientation mode has exactly zero energy, and the $K = 0$ and $K = 2$ modes are degenerate. In the asymmetric case (A), the rational 2:1 ratio of frequencies gives a slightly non self-consistent solution, which results in a $O(1/M)$ stability of the spurious mode and the $K = 0$ and $K = 2$ modes being nondegenerate to the same $O(1/M)$ order. Of course, if the self-consistency condition is imposed, one obtains $I_{21} = 0$ [22] for any nonzero deformation.

TABLE III

Values of I_{2K}^{SD} for $K = 0, 1$, and 2 (in units of $\frac{15}{32\pi}\frac{\omega_3}{\omega_0^4}A$).

K	A	B
0	$2M+3-\frac{1}{2M+3}$	$2M+4$
1	$\frac{30}{2M+3}$	0
2	$2M+3+\frac{3}{2M+3}$	$2M+4$

(iii) **Hyperdeformed case.** Here we consider three positions of the Fermi level (see Fig. 3). The results are presented in Table IV and show the degeneracy pattern analogous to the SD case.

TABLE IV

Values of I_{2K}^{HD} for $K = 0, 1$, and 2 (in units of $\frac{15}{32\pi}\frac{\omega_3}{\omega_0^4}A$).

K	A	B	C
0	$3M + 4 - \frac{2}{3(M+1)}$	$3M + 5 + \frac{2}{3(M+2)}$	$3M + 6$
1	$\frac{5}{M+1}$	$\frac{5}{M+2}$	0
2	$3M + 4 - \frac{2}{M+1}$	$3M + 5 + \frac{2}{M+2}$	$3M + 6$

3.1.2. Octupole modes

(i) **Spherical case.** Here

$$I_{3K}^{\text{sph}} = \frac{35}{8\pi}\frac{1}{\omega_0^4}A > 0\,, \quad K = 0, 1, 2, 3\,. \tag{36}$$

It is seen that the spherical magic harmonic oscillator is *stable* with respect to octupole distortions, and the values of I_{3K} do not depend on M. It is worth noting that the exact result (36) comes from the delicate cancellation between the M-dependent terms. In Ref. [22], where the terms below the $O(M)$ order were neglected, the authors obtained I_{3K}=0 also for the spherical closed-shell systems.

(ii) **Superdeformed case.** Here, the results (Table V) depend on the value of M for $K = 1$. It should be noted that the shells filled in the experimentally observed SD nuclei correspond to values of $M = 2$ or 3. Therefore, this quantum number cannot be treated as asymptotically large, and the results restrained to the $O(M^2)$ or $O(M)$ order could have been misleading.

TABLE V

Values of I_{3K}^{SD} for K=0, 1, 2, and 3 (in units of $\frac{7}{40\pi}\frac{\omega_3^2}{\omega_0^6}A$).

K	A	B
0	37	73
1	$6M^2 + 18M + 45$	$6M^2 + 24M + 80$
2	70	80
3	100	100

(iii) **Hyperdeformed case.** The results are presented in Table VI. Also in this case, the values of I_{3K} depend on M, and the $O(1/M)$ terms cannot be considered negligible.

TABLE VI

Values of I_{3K}^{HD} for $K = 0, 1, 2$, and 3 (in units of $\frac{1}{40\pi}\frac{\omega_3^2}{\omega_0^6}A$).

K	A	B	C
0	$563 - \frac{328}{M+1}$	$563 + \frac{328}{M+2}$	1079
1	$735 - \frac{336}{M+1}$	$735 + \frac{336}{M+2}$	1015
2	$1055 - \frac{80}{M+1}$	$1055 + \frac{80}{M+2}$	1215
3	1575	1575	1575

3.1.3. Hexadecapole modes

(i) **Spherical case.** Here

$$I_{4K}^{\text{sph}} = \frac{189}{256\pi}\frac{1}{\omega_0^5}A(M^3+6M^2+23M+30) > 0\,, \quad K = 0,1,2,3,4\,. \tag{37}$$

It is seen that the spherical magic harmonic oscillator is *stable* with respect to hexadecapole distortions, and the values of I_{4K} strongly depend on M.

(ii) **Superdeformed case.** Here, the results (Table VII) depend on the values of M and K. It should be noted that, for typical values of $M = 2$ or 3, these expressions cannot be truncated to any particular order in M. Also, the fact the odd-K modes depend linearly on M does not mean that these modes are less stable than the even-K modes which are third-order in M. It is seen that within each sequence A and B and up to the $O(M)$ order, the even-K modes are proportional to one another. Moreover, up to the $O(M^2)$ order, these modes are identical in the A and B sequences. On the other hand, up to the $O(1/M)$ order, the odd-K modes are proportional to one another within the sequences, and they differ already in the leading $O(M)$ order between the two sequences.

TABLE VII

Values of I_{4K}^{SD} for $K = 0, 1, 2, 3$, and 4 (in units of $\frac{27}{4480\pi}\frac{\omega_3^3}{\omega_0^8}A$).

K	A	B
0	$378\left(2M^3+9M^2+\frac{1741}{54}M+\frac{1255}{36}-\frac{(1695/4)}{2M+3}\right)$	$378\left(2M^3+12M^2+\frac{1172}{27}M+\frac{1480}{27}\right)$
1	$7620\left(2M+3-\frac{(1063/254)}{2M+3}\right)$	$4105\left(2M+4\right)$
2	$350\left(2M^3+9M^2+\frac{79}{2}M+\frac{183}{4}-\frac{(69/4)}{2M+3}\right)$	$350\left(2M^3+12M^2+50M+68\right)$
3	$9205\left(2M+3-\frac{(747/263)}{2M+3}\right)$	$6720\left(2M+4\right)$
4	$490\left(2M^3+9M^2+\frac{83}{2}M+\frac{195}{4}+\frac{(135/4)}{2M+3}\right)$	$490\left(2M^3+12M^2+46M+60\right)$

(iii) **Hyperdeformed case.** Instead of giving rather lengthy analytic formulae, in the following only the leading-order terms in M are quoted. They read:

$$I_{4K}^{HD} \simeq \frac{27}{1024\pi}\frac{\omega_3^3}{\omega_0^8}AM^3 f_K > 0\,, \tag{38}$$

where $f_K = 583.2, 144, 540$, and 856 for $K = 0, 1, 2$, and 4, respectively (configurations A, B, and C). On the other hand, for the $K = 3$ hexadecapole mode the result is different:

$$I_{43}^{HD} \simeq \frac{27}{1024\pi}\frac{\omega_3^3}{\omega_0^8}AMf_3 > 0\,, \tag{39}$$

where $f_3 = 11907$ for A and B, and $f_3 = 10206$ for C.

3.2. Octupole shell correction in the RHO model

As seen from Tables V and VI, there exists a correlation between the predictions of the geometrical multi-cluster model and the underlying single-particle picture. Namely, for the systems expected to be asymmetric, the value of I_{3K} is small, and it increases for more symmetric multicluster configurations. This result is already quite encouraging. However, since, in all cases, $I_{3K} > 0$, no octupole instability is predicted by the RPA. On the other hand, it is well known that the deformed shell model alone (here: the RHO) is not able to correctly predict the nuclear binding and deformation

energies, since it partly neglects the two-body interaction energy [24]. It is only the fluctuating part of the total energy — the shell-correction — that is reproduced fairly well by the single-particle model.

Since we know that the smooth energy of the harmonic oscillator is a very poor approximation to the liquid drop energy, we should not expect the RPA result discussed above to be very accurate. Consequently, in the next step we calculate the shell-driving force associated with the doubly-stretched octupole interactions.

In the presence of the small perturbing potential, V, the shell correction energy can be written as

$$\delta E_{\text{shell}} = \delta E^{(0)}_{\text{shell}} + \delta E^{(1)}_{\text{shell}} + \delta E^{(2)}_{\text{shell}} + \dots , \tag{40}$$

where $\delta E^{(0)}_{\text{shell}}$ is the unperturbed shell correction energy,

$$\delta E^{(1)}_{\text{shell}} = \sum_{i=1}^{A} V_{ii} - \sum_{i=1}^{\infty} V_{ii}\tilde{n}_i \tag{41}$$

is the first-order correction to δE_{shell} [25], and

$$\delta E^{(2)}_{\text{shell}} = \sum_{i=1}^{A}\sum_{j=A+1}^{\infty} \frac{|V_{ij}|^2}{E_0 - E_{ij}} - \sum_{i=1}^{\infty}\sum_{j=1}^{\infty} \frac{|V_{ij}|^2}{E_0 - E_{ij}}(\tilde{n}_i - \tilde{n}_j) \tag{42}$$

is the second-order contribution to the shell energy (see Appendix A). In Eqs (41)–(42), $\tilde{n}_i$ is the smoothed occupation number of the single-particle state $|i\rangle$ and E_{ij}–E_0 is the particle-hole excitation energy.

For the octupole field, $V = \beta_{3K} Q''_{3K}$, the first-order term (41) vanishes, and the shell driving force is solely determined by the second-order correction, $\delta E^{(2)}_{\text{shell}}$, which is proportional to the square of the corresponding deformation β_{3K},

$$\delta E^{(2)}_{\text{shell}} = C_{3K}\beta^2_{3K} . \tag{43}$$

The shell-energy octupole-stiffness coefficient, C_{3K}, given by Eq. (42) ($V \to Q''_{3K}$), determines the octupole susceptibility of shell energy. If C_{3K} is negative, then there exists a shell force favoring stable deformations. (The liquid drop model energy never favors reflection-asymmetric shapes. This means that stable octupole shapes can only arise from shell effects, *i.e.*, from the shell-driving force.) On the other hand, if C_{3K} is positive, the shell correction tends to restore reflection symmetry.

The results of calculations for C_{30} are displayed in Fig. 5. For the spherical shape (portion a) the octupole-driving shell force is positive, *i.e.*, there

is no tendency to develop stable octupole deformations. The situation at the SD prolate shape is shown in portion (b). For particle numbers representing the asymmetric cases (A) of Fig. 3, C_{30} is negative. For the symmetric cases (B), there is no shell octupole-driving force towards reflection-asymmetric shapes. Finally, the HD case is illustrated in portion (c) of Fig. 5. As expected, for the systems representing the asymmetric case A of Fig. 3, the shell correction decreases with octupole deformations, while no octupole-driving tendency is predicted for the symmetric case C. A similar tendency has also been predicted for the $K \neq 0$ octupole modes and the hexadecapole mode. (For results for the $K \neq 0$ modes, see Refs [26, 27].)

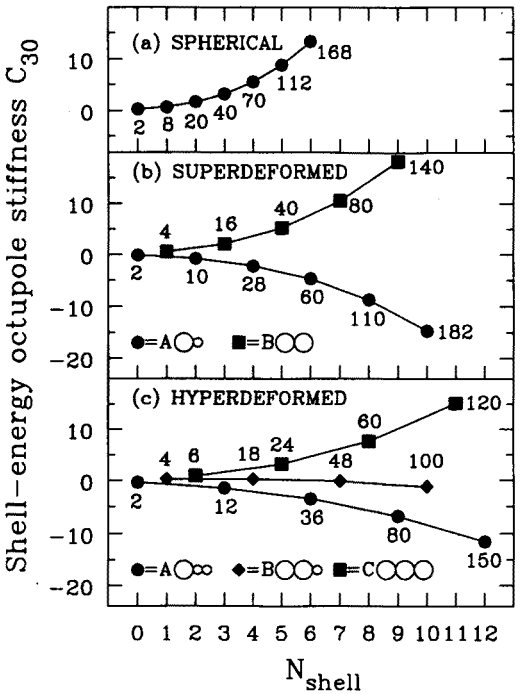

Fig. 5. Shell-correction octupole-stiffness coefficient C_{30} [in units of $7/(4\pi\omega_0^4)$] as a function of the shell quantum number defined as $N_{\rm shell} \equiv n_\perp k_3 + n_3$. Magic particle numbers A (with spin degeneracy included) are indicated for all closed-shell configurations of the RHO at the (a) spherical, (b) superdeformed, and (c) hyperdeformed shape. If C_{30} is negative (positive), then there is (is not) a shell force favoring stable octupole deformations.

The role of spherical clusters in defining properties of SD states becomes more clear when one considers the shell energy of the RHO. For magic numbers given by two unequal spherical clusters (N or Z equal to 28, 60, 110, *etc.*), the shell energy decreases with increasing reflection asymmetry. On

the other hand, for the particle numbers 40, 80, 140, the nuclear shape is expected to be fairly rigid with respect to reflection-asymmetric distortions. (See also Refs [8, 28] for the relation between spherical and SD magic numbers in terms of two touching harmonic oscillators.) For HD shapes, the RHO model suggests that the strongest tendency for reflection asymmetry should be expected in case *A*, *i.e.*, for the particle numbers 12, 36, 80, 150. Particle numbers that stabilize reflection-symmetric shapes (case *C*) are equal to 24, 60, 120.

Calculations based on the realistic mean-field potentials confirm the prediction of the RHO, *i.e.*, regions of particle numbers which favor reflection-symmetric or reflection-asymmetric SD and HD shapes alternate [8, 29]. For SD shapes, the tendency towards mass asymmetry is strongly favored at particle numbers around 28, 64, and 114, while for particle numbers around 38, 84, and 144, the minimum shell-correction energy is found at reflection-symmetric shapes. As far as HD shapes are concerned, the octupole-driving particle numbers are 34, 80, and 150, while the reflection-symmetry-favoring numbers are 22, 58, 104, and 120.

4. Light nuclei

Spectacular examples of multi-cluster configurations have been found and/or predicted in light nuclei. In many cases, these states can be well described in terms of the RHO model. Ikeda *et al.* [30, 31] suggested that multicluster configurations would appear near the threshold energy for decay into the fragments. Figure 6 illustrates this idea using the so-called

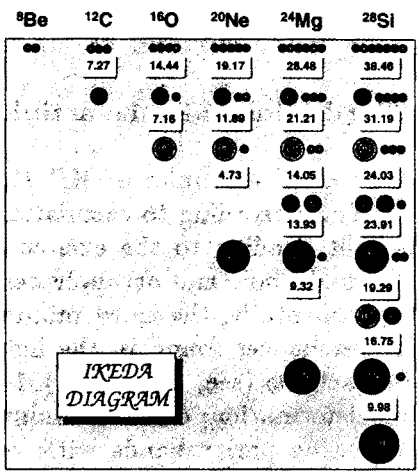

Fig. 6. Ikeda diagram for light nuclei. The threshold energy for each decay mode (in MeV) is indicated. From Ref. [31].

Ikeda diagram. (A detailed discussion of various cluster configurations in light nuclei can be found in Refs [32–34].)

Among many well-deformed configurations in light nuclei, there are several good examples that nicely illustrate the scheme discussed in Sec. 3. For instance:

(i) The SD ground state of ^{8}Be corresponds to two alpha particles side by side. (SD prolate gap at N=2.)

(ii) The ground state of ^{12}C resembles three α-particles in a triangle. This SD oblate shape ($k_1 = k_2 = 2$, $k_3 = 1$) can be associated with the SD oblate gap at $N = 3$. The first excited 0_2^+ level in ^{12}C at 7.65 MeV can be viewed as the HD state (three-α-particle linear cluster; HD prolate gap at $N = 3$).

(iii) The ground state of ^{20}Ne can be well described as arising from an ^{16}O–^{4}He di-nucleus configuration [35–37].

(iv) The 4:1 state in ^{16}O can be described in terms of the four aligned alpha particles [38–40].

(v) The calculated [41] low-lying reflection-asymmetric HD minimum ($\varepsilon_2 = 1, \varepsilon_3 = 0.3$) in ^{24}Mg can be associated with the asymmetric ^{16}O + α+α (or ^{16}O + ^{8}Be) structures, or the symmetric HD α + ^{16}O +α states [42, 43]. (HD prolate gap at $N = 6$.) A six-α chain structure in ^{24}Mg was reported in Ref. [44].

(vi) The ground state of ^{28}Si can be associated with the SD oblate gap occurring for $N = 7$.

(vii) Other examples are the HD states in ^{36}Ar (^{16}O + ^{16}O + α), ^{48}Cr (^{16}O + ^{16}O + ^{16}O) (see discussion in Ref. [45]).

5. Third minima in the actinides

In heavy nuclei, very good examples of HD states are the so-called third minima around ^{232}Th. According to calculations, in these nuclei the second saddle point is split, leading to the excited reflection-asymmetric configuration with large quadrupole and octupole deformations, $\beta_2 \sim 0.90$, $\beta_3 \sim 0.35$ [46–50]. Experimentally, the third minimum is indicated from a microstructure in the resonances found in the light actinides using the (*n,f*), (*t,pf*), and (*d,pf*) reactions (see, *e.g.*, Refs [51–53]). The very large quadrupole and octupole deformations of third minima manifest themselves by the presence of alternating parity bands with very large moments of inertia (≈ 250 MeV^{-1}) built on the same single-particle state [52].

A systematic study of HD states in actinides, using the Nilsson–Strutinsky model [49], yielded very shallow reflection-asymmetric third minima.

The HD states around ^{232}Th also appear in self-consistent calculations based on the Gogny–Hartree–Fock–Bogolyubov model with the D1S interaction [54] and the ATDHF–Skyrme–Yukawa calculation [55].

In Ref. [50], systematic calculations of potential energy surfaces of the even-even Rn, Ra, Th, and U isotopes have been performed using the shell-correction approach with the microscopic energy computed with the axially-deformed Woods–Saxon potential [56] and the macroscopic energy taken from the Yukawa-plus-exponential mass formula of Ref. [57]. The potential energy surfaces were calculated in a many-dimensional deformation space $(\beta_2 - \beta_7)$, allowing for a rather general description of axially-deformed reflection-asymmetric shapes. As an example, Fig. 7 shows the calculated shapes of ^{232}Th in the (β_2, β_3)-plane.

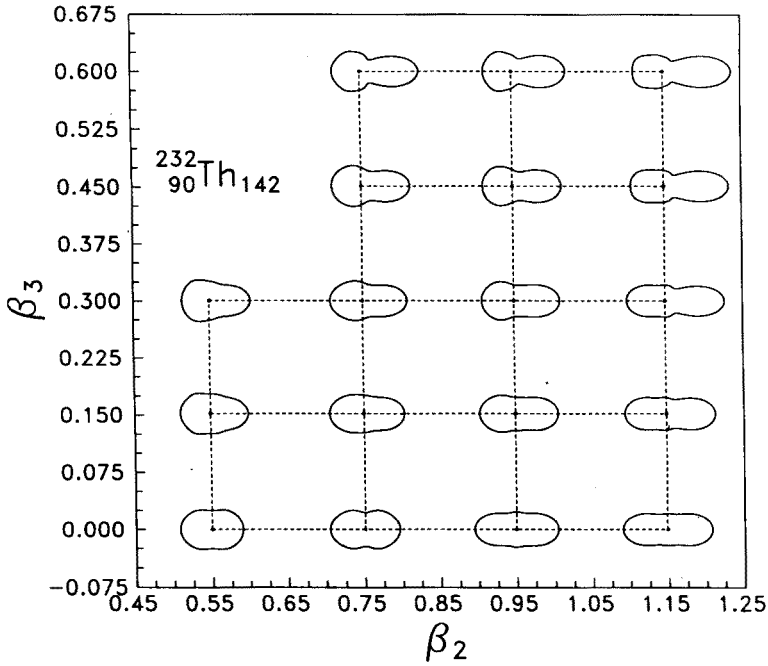

Fig. 7. The shapes of ^{232}Th in the (β_2, β_3)-plane. At each value of β_2 and β_3, the remaining deformations β_4–β_7 were obtained by minimizing the total energy.

According to the Woods–Saxon–Strutinsky calculations, third minima appear in many actinide nuclei. They are characterized by very large elongations ($\beta_2 \sim 0.9$) and significant reflection asymmetry ($0.35 < \beta_3 < 0.65$). Fig. 8 displays the Woods–Saxon potential energy curve (relative to the spherical macroscopic energy) for ^{232}Th as a function of quadrupole deformation, β_2, along the static fission path. Also shown are the macro-

scopic energy and shell correction curves. The very pronounced reflection-asymmetric HD minimum at $\beta_2 = 0.85$ and $\beta_3 = 0.35$ lies about 2 MeV above the (yet unobserved!) reflection-symmetric SD minimum ($\beta_2 = 0.6$) and is separated by ~ 2 MeV barrier. As seen in Fig. 8, the predicted stability of the HD minimum in ^{232}Th comes from the strong shell effect at HD reflection-asymmetric shapes. The very low shell energy partly compensates for the increase in macroscopic energy with deformation.

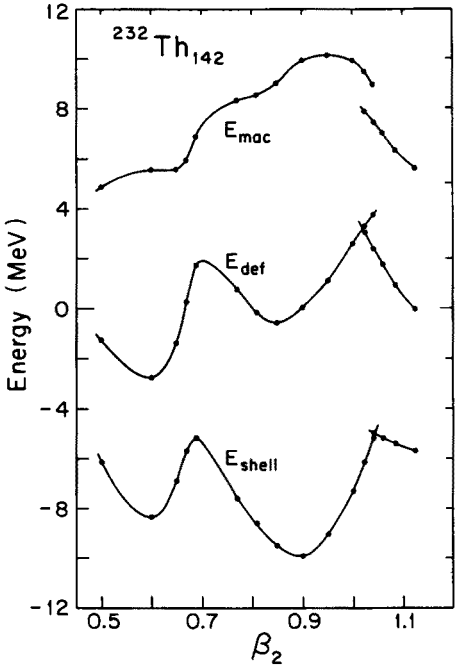

Fig. 8. Macroscopic energy ($E_{\rm mac}$), shell correction ($E_{\rm shell}$), and total energy (relative to the spherical macroscopic energy) ($E_{\rm def} = E_{\rm mac} + E_{\rm shell}$) for ^{232}Th as a function of quadrupole deformation, β_2, along the static fission path.

The PES's in the (β_2, β_3)-plane for several even-even Rn, Ra, Th, and U nuclei are displayed in Fig. 9. The range of quadrupole deformation ($0.55 \leq \beta_2 \leq 1.15$) covers the region between the second minimum and the outer barrier. For all the nuclei shown in Fig. 9, there exist well-developed reflection-asymmetric HD minima. As discussed in Ref. [50], the static fission path shows a pronounced Z and N dependence. Interestingly, in the nuclei around ^{234}U, the HD minimum splits into two distinct minima with very different values of β_λ ($\lambda = 3 - 7$).

The most interesting conclusion of Ref. [50] is that the structure of the third minimum corresponds to a bi-nuclear configuration involving a

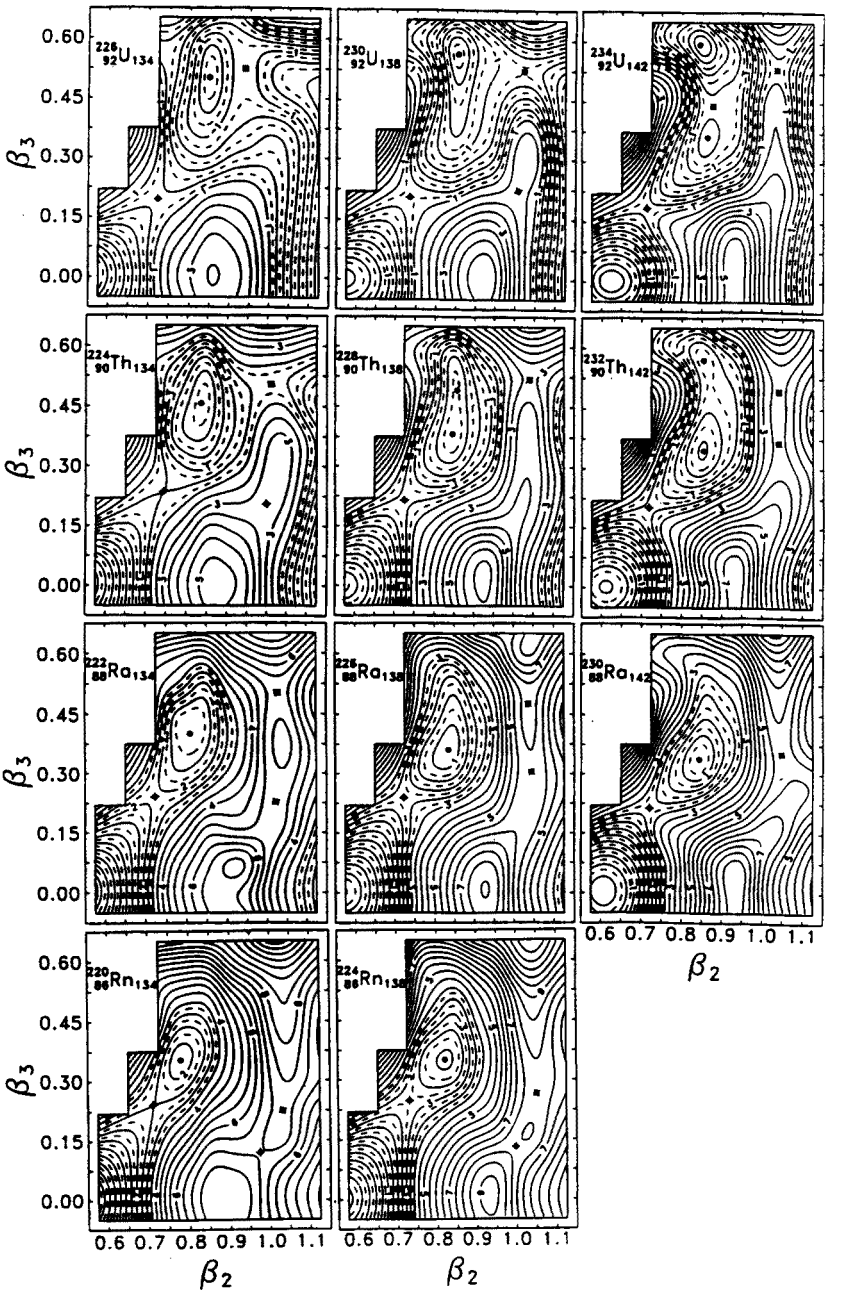

Fig. 9. The Woods–Saxon–Strutinsky total potential energy for ^{220,224}Rn, ^{222,226,230}Ra, ^{224,228,232}Th, and ^{226,230,234}U, as a function of β_2 and β_3. At each (β_2, β_3) point the energy was minimized with respect to $\beta_4 - \beta_7$. The distance between the solid contour lines is 0.5 MeV. The additional dashed contour lines are 0.25 MeV apart. The minima (saddle points) are marked by dots (crossed dots).

spherical (or nearly-spherical) heavy fragment around ^{132}Sn and a well-deformed lighter fragment around ^{100}Zr. This is illustrated in Fig. 10, which shows the predicted equilibrium shapes of ^{232}Th. Indeed, the shape corresponding to the HD minimum looks like a superposition of the ^{132}Sn and ^{100}Zr ground-state shapes. Recently, this result has been confirmed by the calculations of Ref. [58], based on the relativistic mean field theory. The single-particle spectrum of ^{232}Th at the third minimum resembles a situation known from the two-center shell-model calculations, *i.e.*, it can be viewed in terms of combined ground-state spectra of ^{132}Sn (spherical) and ^{100}Zr (deformed) (see Fig. 11).

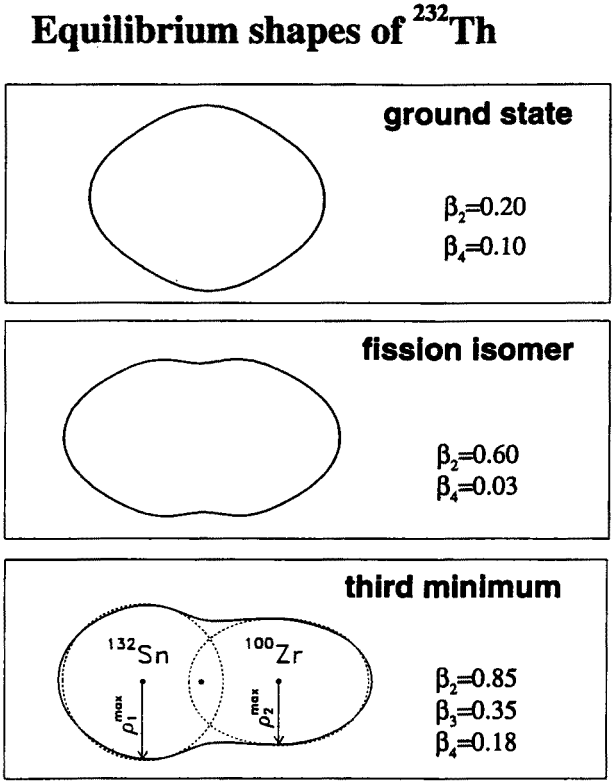

Fig. 10. Calculated equilibrium shapes of ^{232}Th at the ground-state (top), fission-isomeric (middle), and third-minimum (bottom) configuration.

The clustering effect predicted in the third minima is a striking manifestation of nuclear shell structure; in the RHO model the particle numbers 80 and 150 correspond to the situation which formally resembles one spherical doubly-magic fragment and one well-deformed (or SD) lighter fragment. The very special role played by the ^{132}Sn structure in the fission process has been noted before in the context of mass distributions of fission fragments

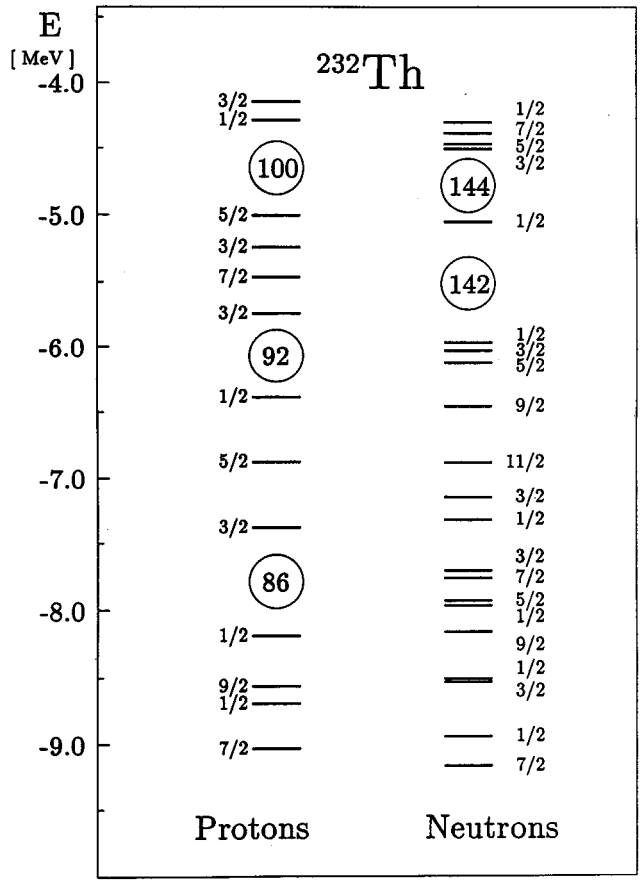

Fig. 11. Single-particle levels of ^{232}Th in the third minimum.

[59] and the recent analysis of cold fission data [60]. Recent measurements of mass and kinetic energy distributions for the photofission of ^{232}Th [61] demonstrate an enhanced yield for masses around 134. This result is consistent with the predicted "bi-nuclear" structure of the HD minimum in ^{232}Th.

6. Conclusions

The clustering phenomenon in atomic nuclei is a direct manifestation of a particularly strong ground-state stability of spherical magic systems. In lighter nuclei, many excited states (resonances) can be explained in terms of multicluster configurations involving ^{4}He, ^{12}C, or ^{16}O. In heavy nuclei, the best examples are the HD minima around ^{232}Th. The strong shell effects associated with multicluster configurations can be qualitatively understood in the RHO model. In this context, two works, namely *(i)* by Bayman

and Bohr on the connection between the cluster model and the SU(3) coupling scheme for particles in a harmonic oscillator potential [62], and *(ii)* by Harvey on the harmonic oscillator approximation for fusion/fission [63], are particularly important.

Oak Ridge National Laboratory is managed for the U.S. Department of Energy by Martin Marietta Energy Systems, Inc. under contract No. DE-AC05-84OR21400. The Joint Institute for Heavy Ion Research has as member institutions the University of Tennessee, Vanderbilt University, and the Oak Ridge National Laboratory; it is supported by the members and by the Department of Energy through Contract No. DE-FG05-87ER40361 with the University of Tennessee. Theoretical nuclear physics research at the University of Tennessee is supported by the U.S. Department of Energy through Contract No. DE-FG05-93ER40770. Work at the University of Pittsburgh was supported by the NSF Pittsburgh-Warsaw collaboration grant No. INT-9115309 and by NSF grant No. PHY-9022196. Some of the calculations were performed at the Pittsburgh Super Computer Center under grant No. PHY900027P. This research was supported in part by the Polish Committee for Scientific Research under Contract No. 20450 91 01.

APPENDIX A

Shell correction energy in the presence of perturbing potential

The shell correction can be calculated by taking the difference between the sum of occupied levels and its average value [25, 64–66],

$$E_{\rm shell} = E_{\rm s.p.} - \tilde{E}_{\rm s.p.} = \sum_{i-{\rm occ}} \epsilon_i - \int_{-\infty}^{\tilde{\lambda}} \epsilon\, \tilde{g}(\epsilon) d\epsilon\,, \tag{44}$$

where $\tilde{\lambda}$ is the smoothed Fermi level defined through the particle number equation:

$$N = \int_{-\infty}^{\tilde{\lambda}} \tilde{g}(\epsilon) d\epsilon\,, \tag{45}$$

and $\tilde{g}(\epsilon)$ is the mean single-particle level density obtained from the single-particle level density (1) by folding with a smoothing function $f(x)$:

$$\tilde{g}(\epsilon) = \frac{1}{\gamma} \int_{-\infty}^{+\infty} d\epsilon' g(\epsilon') f\left(\frac{\epsilon - \epsilon'}{\gamma}\right) = \frac{1}{\gamma} \sum_i f\left(\frac{\epsilon - \epsilon_i}{\gamma}\right) = \frac{1}{\gamma} \sum_i f_i\,. \tag{46}$$

In Eq. (46), γ is the smoothing range; it should be larger than the typical distance between major shells.

The smoothed single-particle energy can be expressed in the form [67]:

$$\tilde{E}_{\mathrm{s.p.}} = \int_{-\infty}^{\tilde{\lambda}} \epsilon\, \tilde{g}(\epsilon) d\epsilon = \sum_i \epsilon_i \tilde{n}_i + \gamma \frac{d\tilde{E}_{\mathrm{s.p.}}}{d\gamma}\,, \tag{47}$$

where the smoothed occupation numbers are

$$\tilde{n}_i = \frac{1}{\gamma} \int_{-\infty}^{\tilde{\lambda}} d\epsilon\, f\left(\frac{\epsilon - \epsilon_i}{\gamma}\right). \tag{48}$$

Since the value of $\tilde{E}_{\mathrm{s.p.}}$ should not depend on the smoothing range γ, the second term in Eq. (47) must vanish, *i.e.*,

$$\tilde{E}_{\mathrm{s.p.}} = \sum_i \epsilon_i \tilde{n}_i\,. \tag{49}$$

In the presence of a small perturbing potential, the single-particle energies are slightly modified, *i.e.*, $\epsilon_i \to \epsilon_i + \delta\epsilon_i$. Following Eq. (49), the corresponding change in the average single-particle energy is:

$$\delta\tilde{E}_{\mathrm{s.p.}} = \tilde{\lambda}\tilde{g}(\tilde{\lambda})\delta\tilde{\lambda} + \int_{-\infty}^{\tilde{\lambda}} \epsilon\, \delta\tilde{g}(\epsilon) d\epsilon\,. \tag{50}$$

The variation $\delta\tilde{\lambda}$ can be calculated from the particle number equation (45),

$$\delta N = 0 \Longrightarrow \tilde{g}(\tilde{\lambda})\delta\tilde{\lambda} + \int_{-\infty}^{\tilde{\lambda}} \delta\tilde{g}(\epsilon) d\epsilon = 0\,. \tag{51}$$

After using the identity

$$\delta\tilde{g}(\epsilon) = \frac{1}{\gamma}\sum_i \frac{\partial f}{\partial \epsilon_i}\delta\epsilon_i = -\frac{1}{\gamma}\sum_i \frac{\partial f_i}{\partial \epsilon}\delta\epsilon_i\,, \tag{52}$$

(folding function depends only on the difference $\epsilon - \epsilon_i$) and combining Eqs. (50), (51), (46), and (48), one obtains

$$\begin{aligned}\delta\tilde{E}_{\mathrm{s.p.}} &= -\int_{-\infty}^{\tilde{\lambda}} (\tilde{\lambda} - \epsilon)\, \delta\tilde{g}(\epsilon) d\epsilon = \frac{1}{\gamma}\sum_i \int_{-\infty}^{\tilde{\lambda}} (\tilde{\lambda} - \epsilon)\, \frac{\partial f_i}{\partial \epsilon}\delta\epsilon_i\, d\epsilon \\ &= \frac{1}{\gamma}\sum_i \delta\epsilon_i \int_{-\infty}^{\tilde{\lambda}} f_i d\epsilon = \sum_i \delta\epsilon_i\, \tilde{n}_i\,.\end{aligned} \tag{53}$$

This result shows that, at variance with the suggestion expressed in Ref. [27], the variation of the smoothed occupation numbers, $\tilde{n}_i$, in Eq. (49) does not contribute to the variation of the average single-particle energy. For this result to be valid, one only has to properly take into account the conservation of the average number of particles.

REFERENCES

[1] A. Bohr, B.R. Mottelson, *Nuclear Structure*, vol. 2, W.A. Benjamin, New York 1975.
[2] R. Balian, C. Bloch, *Ann. Phys.* (NY) **69**, 76 (1971).
[3] V.M. Strutinsky, A.G. Magner, *Sov. J. Part. Nucl.* **7**, 138 (1976).
[4] V.M. Strutinsky, A.G. Magner, S.R. Ofengenden, T. Døssing, *Z. Phys.* **A283**, 269 (1977).
[5] M.C. Gutzwiller, *J. Math. Phys.* **8**, 1979 (1967); *J. Math. Phys.* **12**, 343 (1971).
[6] K. Arita, K. Matsuyanagi, *Prog. Theor. Phys.* **91**, 723 (1994).
[7] I. Ragnarsson, S.G. Nilsson, R.K. Sheline, *Phys. Rep.* **45**, 1 (1978).
[8] T. Bengtsson, M.E. Faber, G. Leander, P. Möller, M. Płoszajczak, I. Ragnarsson, S. Åberg, *Phys. Scripta* **24**, 200 (1981).
[9] C.Y. Wong, *Phys. Lett.* **32B**, 668 (1970).
[10] I. Vendramin, *Nuovo Cim.* **54A**, 190 (1968).
[11] G. Maiella, G. Vilasi, *Lett. Nuovo Cim.* **1**, 57 (1969).
[12] C. Quesne, *J. Phys. A* **19**, 1127 (1986).
[13] F. Duimio, G. Zambotti, *Nuovo Cim.* **48A**, 1203 (1966).
[14] R.A. Brandt, O.W. Greenberg, *J. Math. Phys.* **10**, 1168 (1969).
[15] G. Rosensteel, J.P. Draayer, *J. Phys. A* **22**, 1323 (1989).
[16] W. Nazarewicz, J. Dobaczewski, P. Van Isacker, in: *Future Directions in Nuclear Physics with 4π Gamma Detection Systems*, eds J. Dudek, B. Haas, AIP Conference Proceedings **259**, AIP, New York 1992, p. 30.
[17] W. Nazarewicz, J. Dobaczewski, *Phys. Rev. Lett.* **68**, 154 (1992).
[18] W. Nazarewicz, in: *Recent Advances in Nuclear Structure*, eds D. Bucurescu, G. Cata-Danil, and N.V. Zamfir, World Scientific Publ., 1991, p. 175.
[19] D.G. Ravenhall, R.T. Sharp, W.J. Pardee *Phys. Rev.* **164**, 1950 (1967).
[20] T. Nakatsukasa, S. Mizutori, K. Matsuyanagi, *Prog. Theor. Phys.* **87**, 607 (1992).
[21] R. Nazmitdinov, S. Åberg, *Phys. Lett.* **289B**, 238 (1992).
[22] H. Sakamoto, T. Kishimoto, *Nucl. Phys.* **A501**, 205 (1989).
[23] H. Sakamoto, T. Kishimoto, *Nucl. Phys.* **A501**, 242 (1989).
[24] P. Ring, P. Schuck, *The Nuclear Many-Body Problem*, Springer-Verlag, 1980.
[25] M. Brack, J. Damgård, A.S. Jensen, H.C. Pauli, V.M. Strutinsky, C. Y. Wong, *Rev. Mod. Phys.* **44**, 320 (1972).
[26] W. Nazarewicz, in: *Nuclear Shapes and Nuclear Structure at Low Excitation Energies*, eds M. Vergnes, J. Sauvage, P.-H. Heenen, and H.T. Doung, NATO ASI Series B: Physics, Vol. 289, Plenum Press, 1992, p. 247.

[27] K. Arita, K. Matsuyanagi, *Prog. Theor. Phys.* **89**, 389 (1993).
[28] M. Faber, M. Płoszajczak, *Phys. Scr.* **24**, 189 (1981).
[29] J. Höller, S. Åberg, *Z. Phys.* **A336**, 363 (1990).
[30] K. Ikeda, N. Takigawa, H. Horiuchi, *Prog. Theor. Phys. Suppl.* (Extra Number), 464 (1968).
[31] H. Horiuchi, K. Ikeda, Y. Suzuki, *Suppl. Prog. Theor. Phys.* **52**, 89 (1972).
[32] R.K. Sheline, K. Wildermuth, *Nucl. Phys.* **21**, 196 (1960).
[33] W.D.M. Rae, *Int. J. Mod. Phys.* **A3**, 1343 (1988).
[34] J. Cseh, W. Scheid, *J. Phys. G* **18**, 1419 (1992).
[35] F. Nemoto, H. Bando, *Prog. Theor. Phys.* **47**, 1210 (1972).
[36] S. Marcos, H. Flocard, P.-H. Heenen, *Nucl. Phys.* **A410**, 125 (1083).
[37] D. Provoost, F. Grümmer, K. Goeke, P.-G. Reinhardt, *Nucl. Phys.* **A431**, 139 (1984).
[38] Y. Fujiwara, H. Horiuchi, K. Ikeda, M. Kamimura, K. Sato, Y. Suzuki, E. Uegaki, *Prog. Theor. Phys. Suppl.* **68**, 29 (1980).
[39] S. Åberg, I. Ragnarsson, T. Bengtsson, R.K. Sheline, *Nucl. Phys.* **A391**, 327 (1982).
[40] D. Auverlot, P. Bonche, H. Flocard, P.-H. Heenen, *Phys. Lett.* **149B**, 6 (1984).
[41] G.A. Leander, S.E. Larsson, *Nucl. Phys.* **A239**, 93 (1975).
[42] H. Flocard, P.H. Heenen, S.J. Krieger, M. Weiss, *Prog. Theor. Phys.* **72**, 1000 (1984).
[43] A.S. Umar, M.R. Strayer, R.Y. Cusson, P.-G. Reinhard, D.A. Bromley, *Phys. Rev.* **C32**, 172 (1985).
[44] A.H. Wuosmaa, R.R. Betts, B.B. Back, M. Freer, B.G. Glagola, Th. Happ, D.J. Henderson, P. Wilt, I.G. Bearden, *Phys. Rev. Lett.* **68**, 1295 (1992).
[45] W.D.M. Rae, A.C. Merchant, *Phys. Lett.* **B279**, 207 (1992).
[46] V.V. Pashkevich, *Nucl. Phys.* **A169**, 275 (1971).
[47] P. Möller, *Nucl. Phys.* **A192**, 529 (1972).
[48] P. Möller, J.R. Nix, *Physics and Chemistry of Fission 1973*, IAEA, Vienna 1974, vol. 1, p. 103.
[49] R. Bengtsson, I. Ragnarsson, S. Åberg, A. Gyurkovich, A. Sobiczewski, K. Pomorski, *Nucl. Phys.* **A473**, 77 (1987).
[50] S. Ćwiok, W. Nazarewicz, J.X. Saladin, W. Płóciennik, A. Johnson, *Phys. Lett.* **B 322**, 304 (1994).
[51] B. Fabbro, J. Blons, A. Greiner, J.M. Hisleour, C. Mazur, Y. Patin, D. Paya, M. Ribrag, *J. Phys. Lett.* **45**, L-843 (1984).
[52] J. Blons, *Nucl. Phys.* **A502**, 121c (1989).
[53] Y. Nakagome, R.C. Block, R.E. Slovacek, E.B. Bean, *Phys. Rev.* **C43**, 1824 (1991).
[54] J.F. Berger, M. Girod, D. Gogny, *Nucl. Phys.* **A502**, 85c (1989).
[55] M.K. Pal, *Nucl. Phys.* **A556**, 201 (1993).
[56] S. Ćwiok, J. Dudek, W. Nazarewicz, J. Skalski, T. Werner, *Comput. Phys. Commun.* **46**, 379 (1987).
[57] P. Möller, J.R. Nix, *At. Data Nucl. Data Tables* **39**, 213 (1988).
[58] K. Rutz, J.A. Maruhn, P.-G. Reinhard, W. Greiner, preprint.

[59] B.D. Wilkins, E.P. Steinberg, R.R. Chasman, *Phys. Rev.* **C14**, 1832, (1976).
[60] M. Asghar, N. Boucheneb, G. Medkour, P. Geltenbort, B. Leroux, *Nucl. Phys.* **A560**, 677 (1993).
[61] M. Piessens, E. Jacobs, S. Pommé, D. De Frenne, *Nucl. Phys.* **A556**, 88 (1993).
[62] B. Bayman, A. Bohr, *Nucl. Phys.* **9**, 596 (1958).
[63] M. Harvey, *Phys. Lett.* **24B**, 374 (1967).
[64] W.J. Swiatecki, in: Proc. 2nd Int. Conf. on Nuclidic Masses, Vienna, 1963, ed. by: W.H. Johnson, Jr., Springer-Verlag, Vienna 1964, p. 58.
[65] V.M. Strutinsky, *Nucl. Phys.* **A95**, 420 (1967).
[66] V.M. Strutinsky, *Nucl. Phys.* **A122**, 1 (1968).
[67] M. Brack, H.C. Pauli, *Nucl. Phys.* **A207**, 401 (1973).